Donor-vacancy complexes in Ge: Cluster and supercell calculations

J. Coutinho,[1] S. Öberg,[2] V. J. B. Torres,[1] M. Barroso,[1] R. Jones,[3] and P. R. Briddon[4]
[1]*Department of Physics, University of Aveiro, Campus Santiago, 3810-193 Aveiro, Portugal*
[2]*Department of Mathematics, Luleå University of Technology, Luleå S-97187, Sweden*
[3]*School of Physics, University of Exeter, Exeter EX4 4QL, United Kingdom*
[4]*School of Natural Sciences, University of Newcastle upon Tyne, Newcastle upon Tyne NE1 7RU, United Kingdom*
(Received 20 March 2006; published 26 June 2006)

We present a comprehensive spin-density functional modeling study of the structural and electronic properties of donor-vacancy complexes (PV, AsV, SbV, and BiV) in Ge crystals. Special attention is paid to spurious results which are related to the choice of the boundary conditions (supercell-cluster approach), the resulting band-gap width, and the choice of the points to sample the Brillouin zone. The underestimated energy gap, resulting from the periodic conditions together with the local-density approximation to the exchange-correlation energy, leads to defect-related gap states that are strongly coupled to crystalline states within the center of the zone. This is shown to produce a strong effect even on relative energies. Our results indicate that in all E centers the donor atom occupies a nearly substitutional site, as opposed to the split-vacancy form adopted by the SnV complex in Si. The E centers can occur in four charge states, from positive to double negative, and produce occupancy levels at $E(0/+)=E_v+0.1$ eV, $E(-/0)=E_v+0.3$ eV, and $E(=/-)=E_c-0.3$ eV.

DOI: 10.1103/PhysRevB.73.235213 PACS number(s): 61.72.Bb, 61.80.Az, 71.55.Cn, 71.70.Ej

I. INTRODUCTION

Intrinsic limitations in carrier mobility in Si, together with the recent advances in high-κ dielectrics research, has led to the resurgence of Ge as a key ingredient in a new generation of ultrafast devices to operate in a regime of tens of gigahertz.[1,2] Recent defect studies in Ge are scarce, particularly those dealing with the atomic and electronic details of elemental radiation induced defects. This deficiency applies not only to experimental reports (see Refs. 3, 4, and references therein), but to modeling studies as well.[5–11] In this context, a detailed understanding of the properties of defects in Ge, especially those that may affect device yield and performance, is highly desirable.

The class of vacancy-impurity complexes is particularly important as we know that many substitutional centers (including dopants) migrate by reacting with radiation- or thermally generated vacancies.[12] This also includes the actual Ge atoms in Ge crystals. According to ^{71}Ge tracer-diffusion measurements, self-diffusion in Ge is dominated by a vacancy mechanism.[13,14] This is a major departure from what we know in Si, where self-interstitial mediated self-diffusion plays an important role.[15,16] The importance of vacancies in Ge has been recently highlighted after *ab initio* calculations predicting a formation energy for the single Ge vacancy as low as 1.7–1.9 eV (depending on its charge state).[6] This is considerably less than the 3.55 eV formation energy of a self-interstitial in Ge,[17] and comparably less than that of a vacancy in Si which has been estimated as ~4.4 eV.[18] It also suggests that at 600 °C the concentration of thermal vacancies is about 10^{12} cm^{-3} in Ge, contrasting with much less than one single vacancy per cm^{-3} under similar conditions in Si.

Here, we report on *ab initio* density functional studies of a class of prominent radiation defects in Ge, namely donor-vacancy (DV) complexes (D=P,As,Sb,Bi), also known as E centers, which are responsible for heavy compensation effects in n-Ge crystals subject to MeV irradiation. We pay special attention to the electronic structure of such complexes, as well as to the approximations involved in treating the host crystal, i.e., by using Ge supercells or Ge clusters.

Before summarizing previous experimental and theoretical results concerning the E centers in Ge, it is instructive to present a short description of the analogous centers in Si. Early electron paramagnetic resonance (EPR) experiments on e-irradiated n-doped Si established much of their properties, including an atomic model shown in Fig. 1(a).[19,20] This model is referred to as *full-vacancy* structure here, and we discern it from the *split-vacancy* model shown in Fig. 1(b), which has been assigned to the tin-vacancy complex in Si.[21,22] The E centers in Si are produced by trapping mobile vacancies next to n-dopants. They introduce a deep acceptor state at around $E_c-0.4$ eV, and are stable up to about ~170 °C.[19,23] Three valence electrons from the group-V atom saturate Si atoms i', j', and k', leaving two other electrons in a *lone* pair state below the valence band maximum. In the neutral defect, the Si radicals i, j, and k contribute with a total of three electrons. These hybridize to form a fully occupied $a_1^{\uparrow\downarrow}$ state also lying below the valence band maxi-

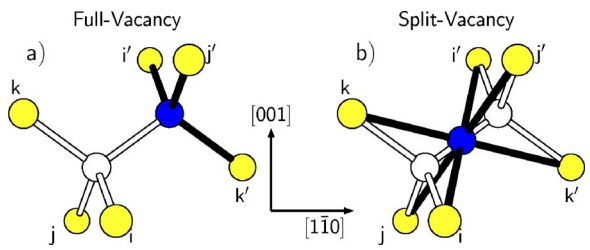

FIG. 1. (Color online) Full-vacancy (a) and split-vacancy (b) atomic models for a donor-vacancy complex in Si and Ge. The donor and host atoms are represented in blue and yellow, respectively. Vacant sites are shown in white.

mum, plus a singly occupied doublet $e^{\uparrow}$ state located within the band gap. According to a simple linear combination of $|i\rangle$, $|j\rangle$, and $|k\rangle$ atomic orbitals (LCAO) centered on *i*, *j*, and *k* radicals, we have

$$\psi_{a_1} = \frac{1}{\sqrt{3}}|i+j+k\rangle, \quad \psi_e = \frac{a}{\sqrt{2}}|i-j\rangle + \frac{b}{\sqrt{6}}|i+j-2k\rangle,$$

with $a^2+b^2=1$. The partial occupancy of the doublet in the neutral state leads to a Jahn-Teller effect which translates into an instability of the trigonal structure against atomic motion. This explains the monoclinic-I pattern of the EPR signal assigned to this complex.[19] In samples doped with P, As, and Sb, the hyperfine data show a large amplitude of the unpaired electron at a *unique* Si atom lying on the mirror plane.[19,20] This is compelling evidence for an $a'^{\uparrow}a''^{0}$ level splitting order on neutral *E* centers in Si (PV^0, AsV^0, and SbV^0). To our knowledge, the assignment of an EPR signal to a BiV^0 complex has not been reported so far.

The above-mentioned model is also supported by stress alignment measurements,[19] which indicate that the center is tensile along the direction perpendicular to the mirror plane. This was interpreted as being consistent with the occupancy of the a' state with bonding character between *i* and *j*, leading to the formation of a weak reconstructed bond between these two Si radicals. Surprisingly, optical absorption combined with uniaxial stress measurements,[20,24] conclude that in the negative charge state the defect is compressive on the plane, and this implies a reversal of the level splitting order to $a''^{\uparrow\downarrow}a'^{0}$.

These features have been accounted for by density functional calculations on hydrogen-terminated Si clusters.[25] Jahn-Teller distortion energies (E_{JT}) of 0.12 and 0.22 eV were calculated for AsV^0 and AsV^-, underestimating the 0.57 and 0.37 eV values from early measurements.[19,20,24] However, the derivation of E_{JT} from experiments has been recently revised,[26] and the figures are now believed to be ~0.18 and ~0.39 eV for AsV^0 and AsV^-, respectively, in much better agreement with theory. Many other theoretical attempts to study the *E* centers in Si have been reported in the literature, particularly dealing with vacancy-assisted diffusion of *n*-dopants and their deactivation upon clustering.[7,12,27–33] All these calculations but those from Ref. 12, which employs the Green's function method, use the supercell approximation to the host Si crystal. Such treatment was often shown to fail in reproducing the observed Jahn-Teller distortions of vacancy-related centers in quantitative and qualitative terms (see, for example, Refs. 33 and 34), and any treatment of the Jahn-Teller effect has been carefully avoided under these circumstances.

Perhaps due to difficulties in performing EPR measurements in Ge, the *E* centers in this material are not as understood as in Si. However, since the mid 1960's the loss of *n*-type conductivity in MeV irradiated Ge crystals has been connected to the formation of these complexes.[35,36] The process is particularly efficient under γ-ray and *e* irradiation,[3,37,38] and in Sb-doped Ge it has been estimated that when the Fermi level is above approximately $E_c-0.2$ eV, the introduction of each SbV defect results in the removal of three free electrons, i.e., the complex has two acceptor states below the Sb donor level.[38] The double-acceptor character of all four *E* centers in Ge was recently reported after deep-level transient spectroscopy (DLTS) and Laplace-DLTS measurements.[3,39,40] First and second acceptor states were located at around $E_v+0.3$ eV and $E_c-0.25$ eV, respectively. Both levels shifted slightly towards the valence band top when increasing the mass of the donor species. Electron emission from the double negatively charged centers was accompanied by a large entropy change, implying that the free energy of ionization depends considerably on the temperature.

Early electrical measurements on γ-ray irradiated *n*-Ge reported the *n-p* conversion after prolonged irradiations.[41] The authors concluded that nearly all donor impurities were converted into acceptor complexes, and these had levels at 0.10, 0.10, 0.12, and 0.16 eV above E_v in crystals doped with P, As, Sb, and Bi, respectively. After type conversion, it was found that the concentration of these acceptors is very low and increases substantially with irradiation dose, up to nearly the initial concentration of group-V impurities. The acceptor nature of the above-mentioned complexes was further supported by the fact that a small concentration of neutral group-III acceptors was detected during electrical measurements at cryogenic temperatures.[41]

Recent DLTS studies in 2 MeV *e*-irradiated Sb-doped Ge-n^+p mesa diodes also investigated the production of a trap at $\sim E_v+0.1$ eV.[42] However, from the electric field dependence of the carrier emission rate, it was concluded that this level is of donor type. Its activation enthalpy was found to be 0.095 eV, and the level anneals out at 85 °C, simultaneously with the disappearance of $SbV(-/0)$ located at $E_v+0.31$ eV.[42]

Clearly, if the Sb-related levels at $\sim E_v+0.1$ eV from Refs. 41 and 42 belong to the same defect, then we need to further investigate this problem and resolve their apparent contradictory conclusions.

Like the experiments, the number of theoretical reports on *ab initio* modeling studies of *E* centers in Ge is rather limited.[7,10,11] Höhler *et al.*[7] report a comprehensive study dealing with vacancy-impurity complexes in Ge. Despite calculating neutral and trigonal defects only, they found that the split-vacancy[43] configuration (DV_{sv}) shown in Fig. 1(b), where the donor atom is located between two *semivacancies*, is the ground state for *D*=Sb and Bi. Accordingly, full-vacancy structures of SbV^0_{fv} and BiV^0_{fv} were found to be unstable, lying 0.64 and 0.86 eV above their ground-state configurations, respectively.[7] On the other hand, ground state PV^0 and AsV^0 defects were found in the full-vacancy form, 0.81 and 0.41 eV below their split-vacancy structures, respectively. We point out that the same work presents an analogous picture for the *E* centers in Si, which cannot be correct. The SbV^0 defect in Si was identified with the monoclinic-I G24 EPR signal in Ref. 20. This signal clearly shows a strong ^{29}Si hyperfine interaction with a *unique* monoclinic Si site where about 60% of the spin density is localized. These data agree only with the Jahn-Teller distorted full-vacancy model.[19,20] In Sec. III we suggest that this discrepancy may derive from the supercell approximation, and one way to minimize the problem will be proposed.

This paper is organized in the following manner. In Sec. II we introduce the calculational details, including the marker method to locate defect levels in the gap. In Secs. III and IV we report defect structures and energetics by using supercells and clusters, respectively. Section V deals with the calculation of electrical levels of several E centers, and finally, the conclusions are given in Sec. VI.

II. THEORETICAL METHOD

We use a spin-density-functional code (AIMPRO),[44] together with a Padé form[45] for the local-density approximation.[46] A Ge crystalline host was simulated either as a cluster of Ge atoms (whose surface was saturated with hydrogen), or as a periodic cubic supercell with 216 Ge atoms. Defect-free clusters are centered at a Ge-Ge bond, D_{3d}-symmetric, spherical in shape, and comprise 396 Ge and 198 H atoms. Both supercells and clusters were produced by assuming the experimental lattice constant of Ge. The H atoms prevent unsaturated surface states from interacting with defect states. The explicit treatment of electronic core states is avoided by using the pseudopotentials of Hartwigsen, Goedecker, and Hutter.[47]

Two types of basis functions are employed to represent the Kohn-Sham states, namely *uncontracted* and *contracted* functions. Uncontracted functions consist of sets of s, p, and d-like atom centered Cartesian-Gaussian orbitals, whose exponents are kept fixed during the self-consistent cycle, but their coefficients are free and independent. For Ge, H, and the group-V species we assigned *ddpp*, *pppp*, and *dddd* basis sets, respectively, where each letter d or p stands for the highest angular momentum of an *spd* set of functions with a particular exponent. For example, Ge atoms have a total of 4 s, 12 p, and 12 d-like functions, whereas for H we have 4 s and 12 p-like functions. For the contracted basis, a set of fixed exponents and contraction coefficients are used to generate a combination of s, p, and d-like functions. A total of four s, four p, and one d-like exponents combined with contraction coefficients were used for Ge. This type of basis is referred to as $44G^*$. Its contraction coefficients were chosen so that the energy per unit cell (E_{cell}), lattice parameter (a_0), bulk modulus (B), and one-electron band structure reproduce the results found with the uncontracted basis, i.e., $E_{\text{cell}}=-217.4509$ eV, $a_0=5.584$ Å, $B=73$ GPa. The lattice parameter and bulk modulus are to be compared with $a_0=5.652$ Å, $B=77$ GPa from measurements.[48,49] Contracted basis are useful without significant loss of accuracy when placed on Ge atoms that are located on bulklike regions.

In cluster calculations, Ge atoms were divided into three regions, namely (i) an inner region made up of five atomic shells (32 Ge atoms) with uncontracted basis; (ii) an intermediate region with contracted basis comprising 15 shells (256 Ge atoms); and (iii) an outer region with 108 Ge atoms bonded to 198 H atoms, both with uncontracted basis. Ge atoms (as well as H atoms) from the outer region are kept locked to their positions during atomic relaxation. Figure 2 depicts the average bond length taken from the four bonds of Ge atoms located on shells 1 to 20, after atomic relaxation of a defect-free cluster. Circles and squares represent data obtained when using the above-mentioned three-region clusters with two Ge basis sets ($44G^*+ddpp$), as well as for a cluster where uncontracted basis functions (*ddpp*) were placed on all Ge atom sites, respectively. Experimental and theoretical (from a periodic calculation) lattice constants are also shown for comparison. It is clear that the atomic displacements are almost insensitive to the basis scheme. The clusters were made by assuming the experimental lattice constant, which leads to an average bond length of about 2.447 Å on the outmost frozen shells. After atomic relaxation the inner bond lengths shrink by at most 0.02 Å, towards the theoretical bond length, and consequently lead to a bond expansion of about 0.01 Å on the intermediate region (shells 8–14). The uncontracted basis calculations tend to result in slightly longer bond lengths. This is a consequence of a small discrepancy (~0.005 Å) between lattice parameters obtained with both basis sets.

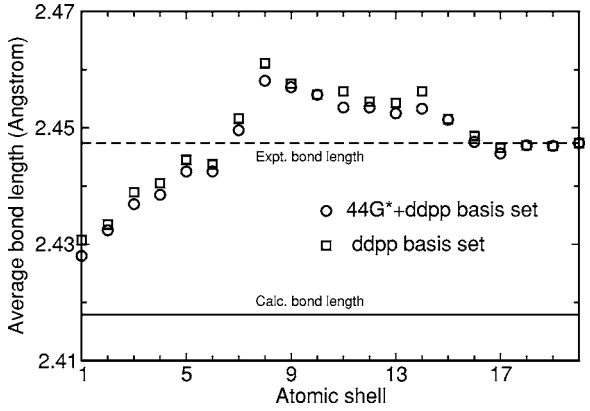

FIG. 2. Bond lengths (Å) between atoms at specific atomic shells in fully relaxed $Ge_{396}H_{198}$ clusters. Only those shells that were allowed to relax are shown (1–20). The experimental and theoretical (from a periodic calculation) bond lengths are represented as dashed and solid horizontal lines, respectively. Squares represent the results when using uncontracted (*ddpp*) basis on all Ge atoms, whereas circles represent the results when using uncontracted basis on the 5 inner shells combined with contracted basis on the next 20 outer shells ($44G^*+ddpp$).

In supercell calculations only uncontracted basis functions were used. The charge density, hartree, and potential energies are dealt in reciprocal space, and to that we employ plane waves of up to 400 Ry kinetic energy. In these calculations, we have to integrate the band structure over the Brillouin zone (BZ). This was carried out according to three schemes, namely (i) at the Γ point; (ii) at a star of 8 special $\mathbf{k}$ points (MP-2^3), properly folded according the symmetry of the cell,[50] and (iii) at the L point located at $\langle 111\rangle \pi/a$, where a is the edge length of the cubic supercell.

The location of the electrical levels was estimated by using the marker method.[51,52] Here, we calculate the electron affinity of, say, a PV defect in a cluster or supercell, $A_{\text{P}}V(-/0)=E(\text{P}V^-)-E(\text{P}V^0)$, where $E(\text{P}V^q)$ is the total energy of the cluster or supercell embedding the defect in charge state q. A charged defect is obtained by adjusting the total number of electrons in the system. For periodic calculations a compensating uniform charge density has to be distributed throughout the cell in order to converge the Coulombic energy.

When no defect is present, the electron affinity of the cluster or supercell, $A(-/0)=E(\mathrm{Ge}^{-})-E(\mathrm{Ge}^{0})$, is the *conduction band* potential (E_c) with respect to the vacuum level, and $A(-/0)-A_{PV}(-/0)$ is the enthalpy for emission of an electron from the acceptor level to the conduction band. Analogously, we can use $I_{PV}(0/+)=E(PV^{0})-E(PV^{+})$ to locate a $PV(0/+)$ donor level. In a defect-free cluster or supercell, $I(0/+)$ is the *valence band* maximum energy (E_v). Hence, the donor level of P*V* is calculated at $E_v+I_{PV}(0/+)-I(0/+)$.

The hydrogen atoms at the cluster surface produce a confining potential which sets the gap of the Ge cluster to $E_g=2.04$ eV.[60] This is almost three times the experimental value, and compromises any calculation of electrical levels on the grounds of the above-mentioned method. On the other hand, it is well known that the local density approximation to the exchange-correlation functional severely underestimates the gap on periodic calculations.[53] Here, we obtain 0.10 and 0.14 eV for direct ($\Gamma_{8v}-\Gamma_{7c}$) and indirect ($\Gamma_{8v}-L_{6c}$) gap transitions, which are to be compared to 0.90 and 0.74 eV measured at 1.5 K.[54] These discrepancies also have consequences for the accuracy of the calculated levels.

Additional problems arise from spurious multipole interactions between a defect and its periodic images in supercell calculations, and several compensating schemes have been proposed in the literature (see, for example, Refs. 55 and 56, and references therein). Considering a standard characteristic supercell size $L\sim 11-17$ Å, we end with dominant monopole corrections of the order of 0.1 eV for first donor states, and ~0.4 eV for second donor states. These errors are unacceptable when dealing with a 0.7 eV gap material.

One way to circumvent these difficulties is to calculate $A(-/0)$ or $I(0/+)$ for a well-characterized defect (marker) with acceptor or donor levels measured at $E_c-\Delta H_m^{\mathrm{exp}}(-/0)$ or $E_v+\Delta H_m^{\mathrm{exp}}(0/+)$, respectively. We may then estimate the error in the calculated acceptor level of the marker,

$$\delta_m^{-/0}=[A(-/0)-A_m(-/0)]-\Delta H_m^{\mathrm{exp}}(-/0),$$

or in the calculated donor level of the marker,

$$\delta_m^{0/+}=[I_m(0/+)-I(0/+)]-\Delta H_m^{\mathrm{exp}}(0/+).$$

Taking again the P*V* center as a case study, and assuming that $\delta_m^{-/0}\approx\delta_{PV}^{-/0}$ and $\delta_m^{0/+}\approx\delta_{PV}^{0/+}$, the enthalpies for electron and hole emission from a P*V* defect may be written as

$$\Delta H_{PV}(-/0)=[A(-/0)-A_{PV}(-/0)]-\delta_{PV}^{-/0},$$

$$\Delta H_{PV}(0/+)=[I_{PV}(0/+)-I(0/+)]-\delta_{PV}^{0/+},$$

or

$$\Delta H_{PV}(-/0)\approx A_m(-/0)-A_{PV}(-/0)+\Delta H_m^{\mathrm{exp}}(-/0),$$

$$\Delta H_{PV}(0/+)\approx I_{PV}(0/+)-I_m(0/+)+\Delta H_m^{\mathrm{exp}}(0/+).$$

The marker method works best when the acceptor or donor states of the marker are similar in symmetry and extent to those of the defect under scrutiny. This condition leads to essentially similar values of $\delta_{PV}^{q-1/q}$ and $\delta_m^{q-1/q}$.[51] The marker method is particularly suitable for supercell calculations where band dispersion effects and strain interactions between the defect and its periodic images are strongly canceled. For this reason, we have chosen the Sb*V* complex as marker. Recent DLTS studies revealed that this defect is responsible for a donor level at $E_v+0.09$ eV, as well as for first and second acceptor states at $E_v+0.31$ eV and $E_c-0.30$ eV, respectively.[40,42]

Let us illustrate how the marker method actually works for a particular case. The cluster results for Sb*V* give $A_{SbV}(-/0)=-3.33$ eV, locating $SbV(-/0)$ at 3.33 eV below the vacuum level. The same calculation for P*V* gives $A_{PV}(-/0)=-3.31$ eV, placing the $PV(-/0)$ level 0.02 eV above $SbV(-/0)$. From Refs. 40 and 42 we know that $SbV(-/0)$ lies at $E_v+0.31$ eV, and hence $PV(-/0)$ is estimated at $E_v+0.33$ eV, i.e., 0.01 eV off the experimental value.

III. SUPERCELL CALCULATIONS

As already pointed out, the Ge gap is severely underestimated under the local density treatment of the exchange-correlation potential.[53] This poses a serious problem when we aim at studying gap levels produced by defects. Supercell calculations invariably sample the band structure over a set of special **k** points in the Brillouin zone. This is often done according to the scheme proposed by Monkhorst and Pack,[50] which is referred to as MP-n^3 and uses a uniform grid of n^3 points. Because degenerate levels may split away from Γ, estimation of Jahn-Teller energies is not reliable when using MP sets with $n>1$. However, in a cubic zone there are two high-symmetry points where the Hamiltonian is real, and where full multiplet structure is available. These are $\mathbf{k}=\Gamma$ and $\mathbf{k}=L=\langle 111\rangle\pi/a$, with a being the edge length of the cell.

Figure 3(a) depicts the one-electron band structure of Ge obtained from the Kohn-Sham eigenvalues along [111] and $[\bar{1}\bar{1}\bar{1}]$ directions in a 216 Ge atom supercell with $a=3a_0$. Only conduction band minimum and valence band maximum bands are shown, and these limit the red hatched areas. The white area in Fig. 3(b) represents the variation of the gap at the **k**-points of interest for the present study. If a trigonal Sb*V* defect aligned along [111] is placed in the cubic cell, the MP-2^3 **k** point grid reduces to $\mathbf{k}_1^*=\langle 111\rangle\pi/6a_0$ and three equivalent points at $\mathbf{k}_2^*=\langle 1\bar{1}\bar{1}\rangle\pi/6a_0$, $\langle\bar{1}1\bar{1}\rangle\pi/6a_0$, and $\langle\bar{1}\bar{1}1\rangle\pi/6a_0$.[61] These are represented as vertical lines in Fig. 3(a), and the direct gap at $\mathbf{k}_1^*$ and $\mathbf{k}_2^*$ is ~0.4 eV.

As mentioned in the Introduction, the three Ge radicals of a trigonal *E* center give rise to a singly occupied *e* level lying in the gap, plus a fully occupied a_1 level below the valence band top. In a supercell calculation, *e* and a_1 levels are associated with doubly degenerate and nondegenerate bands. The latter lies well below E_v and will be disregarded. Doubly degenerate defect bands from full-vacancy and split-vacancy Sb*V* defects in a 216 atom cell are represented in Fig. 3(a) as solid and dashed lines, respectively. Note that each defect band along [111] is doubly degenerate, and their occupancy for the neutral charge state is represented in Fig. 3(b). This

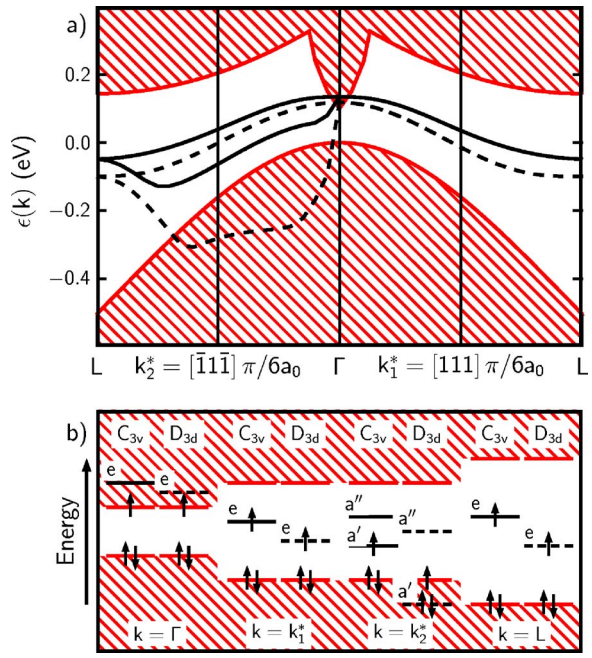

FIG. 3. (Color online) (a) Kohn-Sham band structure of a perfect 216 Ge atom supercell (red hatched area), along with the defect-related band arising from C_{3v}-symmetric (solid black line) and D_{3d}-symmetric (dashed black line) SbV^0 complexes aligned along [111]. (b) Schematic representation of the one-electron filling at relevant **k** points for neutral SbV defects. Only the lowest unoccupied and the highest occupied bulk states (thick red lines) are explicitly shown. Other states related to the SbV complex are resonant with the host density of states. The band structure is represented from $L=[111]\pi/2a_0$ to $L=[\bar{1}\bar{1}\bar{1}]\pi/2a_0$, through $\mathbf{k}_1^*$ and $\mathbf{k}_2^*$ special **k** points from the MP-2^3 sampling grid.

figure makes clear that Γ is not a good sampling point as the e state lies above the conduction band minimum. Consequently, in SbV^0 the paramagnetic electron drops to the conduction band bottom, and the defect is effectively ionized.

Inspection of the wave function of the defect state at $\mathbf{k}_2^*$ shows two difficulties that prevent us from relying on MP schemes to sample the BZ. (i) For a neutral SbV_{fv} with C_{3v} symmetry, the highest occupied state (low-energy branch of the defect band) is strongly mixed with the valence band states. This is shown in Fig. 3(a) by their similar dispersion curvatures around $\mathbf{k}_2^*$. Consequently, the gap state is highly delocalized and spans the entire supercell volume. (ii) For the SbV_{sv} structure with D_{3d} symmetry, most of the low-energy branch of the defect band lies below the valence band top, and the defect is effectively in the negative charge state. Figure 3(b) shows that at $\mathbf{k}_2^*$ the SbV_{sv} defect (D_{3d}) has its doublet split into a' and a'' states, with the former being fully occupied. This means that under these circumstances the center will be effectively in the negative charge state.

Alternatively, at $\mathbf{k}=L$ the gap is about 0.6 eV; defect states lie about midgap and are strongly localized on the Ge dangling bonds. This is certainly not a dense set of **k** points, but as we shall see, it may provide a compromise solution.

In Table I we report the energy difference $E_{\mathrm{sv}}-E_{\mathrm{fv}}$, between split-vacancy and full-vacancy structures. Supercell calculations using Γ, MP-2^3, and L sampling points are compared along with cluster results. All defects have trigonal symmetry, i.e., atomic relaxations were subject to a symmetry constraint. From Table I we note that in general, the larger the direct gap involved in the calculation, the larger the $E_{\mathrm{sv}}-E_{\mathrm{fv}}$ energies. In Γ-point and MP-2^3 calculations, the mixing between defect and crystalline states leads to $E_{\mathrm{sv}}-E_{\mathrm{fv}}$ figures which are weakly sensitive to the charge state. The effect may be understood with help of Fig. 3(b), and is particularly severe for Γ sampling. That figure shows that SbV^+, SbV^0, SbV^-, and Sb$V^=$ will possess an empty e level, while conduction band states will be filled up with electrons. A similar effect takes place at $\mathbf{k}_2^*$, but now the defect bands are strongly mixed with the valence band. We note that at $\mathbf{k}_1^*$ defect levels are well within the gap. Therefore, the consequences of band mixing at the MP-2^3 points are not as severe as in Γ-point calculations. A charge density plot of defect states at $\mathbf{k}_2^*$ allowed us to conclude that they are rather delocalized over the supercell volume.

On the other hand, defect gap states at $\mathbf{k}=L$ are strongly localized at Ge$_i$, Ge$_j$, and Ge$_k$ atoms, and the supercell results are closer to the cluster calculations. This shows how careful we have to be when it comes to the choice of the sampling scheme for this type of periodic calculation. The cluster calculations give even higher $E_{\mathrm{sv}}-E_{\mathrm{fv}}$ values, and we believe that this is a consequence of the overestimated gap width. In order to assess the convergence of the periodic calculations with the size of the supercell (and consequently with the Brillouin zone sampling), we had a look at $E_{\mathrm{sv}}-E_{\mathrm{fv}}$ for SbV on 512 atom supercells with L sampling and *ddpp* basis on all Ge atoms. These calculations give 0.23 and 0.14 eV for

TABLE I. Energy difference ($E_{\mathrm{fv}}-E_{\mathrm{sv}}$), between split-vacancy and full-vacancy E centers in Ge in charge states of interest (in eV). The results were obtained from cluster calculations, and supercell calculations with the Γ point, MP-2^3, and L-point schemes to sample the BZ. In all calculations the full-vacancy defects have a lower total energy.

	PV				AsV		SbV				BiV	
Charge	Γ	MP-2^3	L	Cluster	L	Cluster	Γ	MP-2^3	L	Cluster	L	Cluster
+	0.86	0.83	1.21	1.66	0.73	1.10	0.08	0.05	0.28	0.38	0.17	0.35
0	0.86	0.83	1.11	1.51	0.66	0.99	0.10	0.08	0.22	0.23	0.06	0.17
−	0.85	0.82	1.00	1.32	0.61	0.84	0.10	0.10	0.18	0.18	0.06	0.16
=	0.85	0.76	0.90	1.04	0.53	0.62	0.14	0.11	0.13	0.08	0.05	0.08

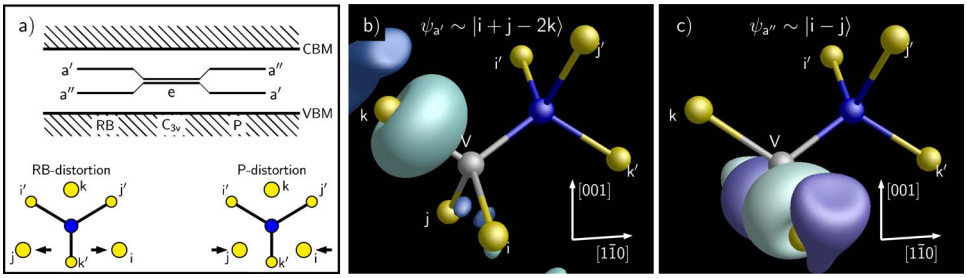

FIG. 4. (Color online) One-electron energy level ordering of an E center in Ge under resonant-bonding (RB), C_{3v}, and pairing (P) distortions, together with diagrams showing the atomic distortions (a). Gap states of the E center, $\psi_{a'}$ and $\psi_{a''}$, represented in (b) and (c), respectively. CBM and VBM in (a) stand for conduction band minimum and valence band maximum, respectively.

SbV^0 and SbV^-, and are to be compared to 0.22 and 0.18 eV, respectively, which were obtained by using 216 atom cells. All these results do not agree with previous calculations suggesting that SbV and BiV occur in a split-vacancy form.[7]

The high-symmetry character of the L point in the BZ not only leads to strongly localized defect states in the gap, but also presents us with a real Hamiltonian. This means that level degeneracy is recovered [see Fig. 3(a)], and we are able to estimate the Jahn-Teller relaxation energies using the supercell approach. A monoclinic distortion splits the e state into $a'+a''$. This is shown in Fig. 4(a). If the distortion is compressive, a bonding state $\psi_{a'}$ between Ge_i and Ge_j lies below $\psi_{a''}$, resulting in a shortening of the Ge_i-Ge_j distance. This is commonly referred as *pairing* (P) distortion,[19] and the neutral charge state has an unpaired electron strongly localized on the Ge_k radical [see Fig. 4(b)]. On the contrary, if the distortion is tensile, an antibonding state $\psi_{a''}$ between Ge_i and Ge_j is occupied, and the Ge_i-Ge_j distance is greater that Ge_i-Ge_k. This is referred as *resonant-bonding* (RB) distortion,[57] and the neutral defect has an unpaired electron on a nodal state as shown in Fig. 4(c).

Three coordinates are chosen to characterize the structure of the E centers, namely Q_{JT}, l, and Q_D, standing for the Jahn-Teller coordinate, the mean distance between radicals, and the *donor distortion* coordinate, respectively. These are defined as

$$Q_{\mathrm{JT}} = \frac{r_{ij} - l}{l}, \quad Q_D = \frac{2r_D}{r_0},$$

with

$$l = (r_{ij} + 2r_{ik})/3,$$

where r_{ij} is the separation between Ge_i and Ge_j atoms, r_0 is the nearest-neighbor Ge-Ge distance, and r_D the displacement of the donor atom from the substitutional site towards the bond-centered site. In supercell calculations, we consider the experimental lattice constant, r_0=2.447 Å, whereas in cluster calculations r_0=2.439 Å, which is the Ge-Ge distance at the center of the relaxed defect-free cluster. Q_D is a fractional displacement of the donor atom, ranging from Q_D=0 (D atom lying at the substitutional site), up to Q_D=1 (where the defect takes the split-vacancy form). For trigonal structures Q_{JT}=0 and l=r_{ij}=r_{ik}.

The electronic ground-state configurations of DV^+, DV^0, DV^-, and $DV^=$ complexes were found to possess a total spin S=0, 1/2, 1, and 1/2, showing C_{3v}, C_{1h}, C_{3v}, and C_{1h} symmetric structures, respectively. Table II shows the relevant structural details of trigonal DV^+ and DV^- defects. These complexes suffer a compressive volumetric relaxation. Values of l are compressed with respect to bulk by ~0.2 and 0.5 Å for DV^+ and DV^-, respectively. These isotropic distortions are only 0.1 Å stronger than those obtained using the cluster calculations. The location of the donor atom is also reported in Table II. Again, displacements Q_D from supercell calculations are slightly larger than those from cluster results. Whereas the donor atom is displaced by $r_D \approx 0.07$, 0.2, 0.4, 0.7 Å for PV, AsV, SbV, and BiV defects in a supercell, cluster calculations give $r_D \approx 0.03$, 0.1, 0.2, and 0.3 Å, respectively. These displacements are rather far from the $r_D \approx 1.2$ Å for a split-vacancy structure.

Neutral and doubly negative DV complexes with C_{3v} symmetry possess a partially occupied doublet state (with 1 and 3 electrons, respectively). This implies that this structure is unstable against a Jahn-Teller distortion. Monoclinic distortions leading to resonant bonding ($r_{ij} > l$) and pairing ($r_{ij} < l$) structures were investigated. Despite starting struc-

TABLE II. Structural details of full-vacancy E centers in Ge with C_{3v} symmetry. Positive and negative charge states have spin-0 and spin-1 ground states, respectively. It also reports the mean distance, l, between Ge radicals (in Å), as well as the donor distortion coordinate Q_{D} (see the text). The nearest-neighbor and second-nearest-neighbor distances at the center of a defect-free cluster (supercell) are r_0=2.439 Å (2.447 Å) and l_0=3.986 Å (3.995 Å), respectively.

	Supercell		Cluster	
Defect	l	Q_D	l	Q_D
PV^+	3.715	0.054	3.853	0.048
PV^-	3.445	0.060	3.498	0.070
AsV^+	3.731	0.162	3.828	0.154
AsV^-	3.459	0.182	3.522	0.182
SbV^+	3.779	0.324	3.877	0.268
SbV^-	3.516	0.344	3.551	0.302
BiV^+	3.856	0.538	3.904	0.418
BiV^-	3.664	0.558	3.647	0.460

TABLE III. Structural details of stable JT distorted (neutral and double-minus charge states) E centers in Ge clusters. It includes the bond distance between Ge_i and Ge_j, r_{ij} (in Å), the mean distance (in Å) between Ge radicals, l, donor distortion coordinate Q_D, JT coordinate Q_{JT}, and JT relaxation energy E_{JT} (in eV). The nearest-neighbor and second-nearest-neighbor distances at the center of a defect-free cluster are $r_0 = 2.4387$ Å and $L_0 = 3.9863$ Å, respectively. NS stands for not stable.

	Resonant bonding					Pairing				
Defect	r_{ij}	l	Q_D	Q_{JT}	E_{JT}	r_{ij}	l	Q_D	Q_{JT}	E_{JT}
PV^0			NS			3.372	3.603	0.052	−0.064	44
P$V^=$			NS			3.227	3.319	0.088	−0.028	39
AsV^0			NS			3.368	3.611	0.158	−0.067	38
As$V^=$			NS			3.272	3.352	0.202	−0.022	37
SbV^0	3.807	3.678	0.284	0.035	48	3.434	3.653	0.282	−0.060	56
Sb$V^=$	3.487	3.411	0.358	0.022	31	3.350	3.412	0.354	−0.018	31
BiV^0	3.861	3.765	0.432	0.026	37	3.597	3.753	0.434	−0.042	39
Bi$V^=$	3.562	3.522	0.508	0.011	24	3.498	3.542	0.522	−0.012	24

tural optimizations with configurations possessing $-0.3 \leq Q_{JT} \leq +0.3$, no meaningful distortions were found upon atomic relaxation. Only PV^0 and AsV^0 exhibit tiny pairing distortions with $Q_{JT} \approx -0.003$, which correspond to a structural relaxation energy $E_{JT} < 2$ meV with respect to the trigonal defect. These figures are certainly smaller than the error bars of the method, and all we can conclude is about the smallness of these distortions in Ge when compared to Si. Remember that the experimental estimates of E_{JT} for AsV^0 and AsV^- in Si are ~0.18 and ~0.39 eV.

IV. CLUSTER CALCULATIONS

Now we discuss the results from cluster calculations. Table I shows that $E_{sv} - E_{fv}$ decreases by ~0.6–0.3 eV when going from DV^+ to $DV^=$, and also decreases by 1.3–1.0 eV from PV to BiV. Clearly, PV and AsV full-vacancy structures are very stable where $E_{sv} - E_{fv} > 0.6$ eV. This energy difference is smaller for SbV and BiV, especially in the double-negative charge state where it is less than 0.1 eV. If we assume an atomic jump frequency attempt of $\sim 10^{13}$ s^{-1} at $T = \infty$, we conclude that even at $T = 80$ K the rate of thermally activated jumps between the two ⟨111⟩-aligned full-vacancy structures will be $\sim 10^8$ s^{-1} for Sb$V^=$ and Bi$V^=$ complexes. This may have consequences for experiments, especially for DLTS where carrier emission peaks are scanned over a scale of up to a few hundred kelvin. If the reorientation rate of the defect becomes much faster than the carrier emission rate, a *thermal-averaged* signal arising from all accessible defect alignments will be observed (see, for example, Ref. 58).

In Table III we report the structural details of Jahn-Teller distorted full-vacancy DV complexes from cluster calculations. In line with the supercell results, DV^+, DV^0, DV^-, and $DV^=$ have ground-state structures with C_{3v}, C_{1h}, C_{3v}, and C_{1h}, respectively.

In the positive charge state, the e state is empty [see Fig. 4(a)] and the defects adopt a perfectly trigonal structure. The distance separating the three pairs of Ge radicals is about 0.1 Å shorter than in bulk, and the P, As, Sb, and Bi atoms are displaced from the substitutional site towards the neighboring vacancy site by about 5, 15, 27, and 42% of half the nearest-neighbor distance, $r_0/2$ (see Table II), respectively. Also in agreement with the supercell results, negatively charged defects were found with a spin-1 ground state and C_{3v} symmetry. In DV^-, Ge radical distances are shortened with respect to bulk values by ~10% and the donor atom displacement from the substitutional site, r_D, varies between 0.1 and 0.8 Å. This corresponds to about 7 to 46% of $r_0/2$. Monoclinic (C_{1h}) DV^- defects with $S=0$ were found to be metastable by 57, 68, 60, and 53 meV for D=P, As, Sb, and Bi, respectively.

Neutral and double negatively charged PV and AsV centers are not stable in a resonant bonding configuration. They spontaneously attain the pairing structure upon atomic relaxation. On the other hand, in these charge states SbV and BiV centers are bistable. Here, relative energies of resonant bonding and pairing configurations are effectively degenerate and they are separated by a potential barrier as low as E_{JT} ~50 meV. It means that both configurations are accessible at cryogenic temperatures. Resonant-bonding DV^0 and $DV^=$ centers show $a''^{\uparrow}$ and $a''^{\uparrow}a'^{\uparrow}$ electronic configurations, respectively. The highest occupied states are similar in shape to those represented in Figs. 4(b) and 4(c). The higher occupancy of a'' results in a small net repulsive interaction between Ge_i and Ge_j, the defect relaxes by $E_{JT} \sim 25-48$ meV, andr_{ij} distances are slightly longer (by 1–4%) than l.

Similar conclusions may be drawn for the pairing structures. Now DV^0 and $DV^=$ possess $a'^{\uparrow}$ and $a'^{\uparrow\downarrow}a''^{\uparrow}$ electronic structures, respectively, and the higher occupancy of the a' state results in a bonding interaction between Ge_i and Ge_j. The Jahn-Teller energy gain is about $E_{JT} \sim 24-56$ meV, and the r_{ij} distances are reduced by 1–7% with respect to l.

It is interesting to note that the configurational space that is accessible by P$V^=$, As$V^=$, and especially Sb$V^=$ and Bi$V^=$ is considerably larger than that for negatively charged states. The latter have a unique C_{3v} orientation. The monoclinic Sb$V^=$ and Bi$V^=$ structures can easily hop within a total of 12 C_{1h} configurations,[59] whereas P$V^=$ and As$V^=$ can jump between three equivalent Jahn-Teller distorted configurations.

TABLE IV. Calculated levels of *E* centers in Ge. Enthalpies and free energies of ionization (ΔH and ΔG), as well as activation energies for carrier emission (ΔE) from Hall-effect (HE) and DLTS measurements are shown for comparison. The levels in the table are reported with respect to the valence band top (*h*-subscripted for hole emission), and to the conduction band minimum (*e*-subscripted for electron emission). All values are in eV.

		P*V*	As*V*	Sb*V*	Bi*V*
CL	$\Delta H_h(0/+)$	0.12	0.11	0.09	0.10
SC	$\Delta H_h(0/+)$	0.07	0.07	0.09	0.10
HE[a]	$\Delta G_h(0/+)$	0.10	0.10	0.12	0.16
DLTS[b]	$\Delta H_h(0/+)$			0.09	
CL	$\Delta H_h(-/0)$	0.33	0.31	0.31	0.29
SC	$\Delta H_h(-/0)$	0.33	0.32	0.31	0.29
DLTS[b]	$\Delta H_h(-/0)$			0.31	
DLTS[c,d]	$\Delta E_h(-/0)$	0.34	0.33	0.30	0.30
CL	$\Delta H_e(=/-)$	0.24	0.25	0.29	0.30
SC	$\Delta H_e(=/-)$	0.30	0.30	0.29	0.28
DLTS[c]	$\Delta H_e(=/-)$	0.22	0.24	0.29	0.26
DLTS[d]	$\Delta E_e(=/-)$			0.37	
DLTS[e]	$\Delta E_e(=/-)$		0.31	0.41	

[a]Emtsev *et al.* (Ref. 41).
[b]Lindberg *et al.* (Ref. 42).
[c]Markevich *et al.* (Ref. 40).
[d]Fage-Pedersen *et al.* (Ref. 3).
[e]Colder *et al.* (Ref. 37).

This could contribute to the large entropy changes ($\Delta S \sim 2-4\ k_B$) that were reported to occur during the $DV(=/-)$ transitions.

V. ELECTRICAL LEVELS

As mentioned in Sec. II, electrical levels of *DV* complexes were calculated by comparing their electron affinities and ionization energies to the same quantities for the Sb*V* complex. The level location is then offset by experimental data related to Sb*V*.[40,42] Table IV reports the positions of $(0/+)$, $(-/0)$, and $(=/-)$ levels for all *E* centers calculated by using *L*-point sampled supercell (SC) and cluster (CL) methods. Hall effect and DLTS data are also shown for comparison. Ionization enthalpies and free energies (ΔH and ΔG) and activation energy (ΔE) for carrier emission (indexed by *e* for electrons and *h* for holes) are reported with respect to the valence band top (for hole emission), or with respect to the conduction band bottom (for electron emission). A consequence of choosing Sb*V* as a marker is that its calculated levels are identical to the measurements.

From the cluster calculations, ionization energies of P*V*, As*V*, Sb*V* and Bi*V* are $I(0/+)=-4.56$, -4.57, -4.59, and -4.58 eV. Offsetting these energies by $-I_{SbV}(0/+) + \Delta H^{exp}_{SbV}(0/+)=4.59+0.09$ eV, we locate P*V*$(0/+)$, As*V*$(0/+)$, and Bi*V*$(0/+)$ at 0.12, 0.11, and 0.10 eV above E_v. Analogously, from the supercell calculations we have $I(0/+)=5.35$, 5.35, 5.37, and 5.38 eV for P*V*, As*V*, Sb*V*, and Bi*V*. Ionization potentials are now positive, which is a consequence of the ill-defined vacuum level in periodic calculations. From the ionization potentials, P*V*$(0/+)$ lies 0.02 eV below Sb*V*$(0/+)$, i.e., at $E_v+0.07$ eV. Similarly, for As*V* and Bi*V* we obtain donor levels at $E_v+0.07$ and $E_v+0.10$ eV, respectively. Both supercell and cluster results suggest that all *E* centers should produce a donor level at $\sim$0.1 eV above the valence band top. Hence, the *E* center related levels from Hall effect measurements,[41] are most likely to be of donor type and not of acceptor type as it was proposed.

Acceptor levels have also been investigated. The cluster results give $A(-/0)=-3.31$, -3.33, -3.33, and -3.35 eV for P*V*, As*V*, Sb*V*, and Bi*V*, respectively. It means that the acceptor levels of all *E* centers are close by, and the heavier the donor impurity the deeper the $(-/0)$ level (with respect to E_c). These electron affinities tell us that P*V*$(-/0)$ lies 0.02 eV above Sb*V*$(-/0)$, that As*V*$(-/0)$ has the same location in the gap as Sb*V*$(-/0)$, and Bi*V*$(-/0)$ is estimated at 0.02 eV below Sb*V*$(-/0)$. Now, assuming Sb*V* as the marker with an acceptor state at $E_v+0.31$ eV, P*V*$(-/0)$, As*V*$(-/0)$, and Bi*V*$(-/0)$ levels are placed at $E_v+0.33$ eV, $E_v+0.31$ eV, and $E_v+0.29$ eV. Identical results were obtained with the supercell method. Electron affinities $A(-/0)=5.37$, 5.38, 5.39, and 5.41 eV were obtained for P*V*, As*V*, Sb*V*, and Bi*V*, placing $(-/0)$ levels at $E_v+0.33$ eV, $E_v+0.32$ eV, $E_v+0.31$ eV, and $E_v+0.29$ eV, respectively. These are only a few tenths of an electron-volt away from the measurements, and mirror the identical character of the acceptor states involved in all centers.

Identical analysis has been done for second acceptor levels. Here, we deal with second electron affinities, $A(=/-)$, and from the cluster calculations we obtain $A(=/-)=-1.98$, -1.99, -2.03, and -2.04 eV for P*V*, As*V*, Sb*V*, and Bi*V*, respectively. Therefore, taking the Sb*V*$(=/-)$ marker level at $E_c-0.29$ eV, we place the P*V*$(=/-)$, As*V*$(=/-)$, and Bi*V*$(=/-)$ levels at 0.24, 0.25, and 0.30 eV below E_c, respectively. Alternatively, the supercell calculations give $A(=/-)=5.42$, 5.42, 5.43, and 5.44 eV, placing the $(=/-)$ levels of P*V*, As*V*, and Bi*V* at 0.30, 0.30, and 0.28 eV below E_c.

VI. CONCLUSIONS

We report on density-functional studies of vacancy-donor pairs in germanium. Their electronic and structural properties are described in detail, and are compared to previous theoretical and experimental results. By starting from what has been learned with the *E* center in Si, it is realized that many properties of these complexes in Ge are distinct and peculiar.

Although the one-electron structures of trigonal *E* centers in Si and Ge are similar, i.e., neutral defects produce a singly occupied doublet state deep in the gap, they become essentially different upon atomic and spin relaxation. Perhaps due to its higher metallic character, JT distortions and energies are much smaller in Ge. Whereas in Si the *E* centers show JT relaxation energies of a few tenths of an electron-volt, in Ge they are in general smaller than 50 meV. In the neutral and double-negative charge states, the lighter P*V* and As*V* complexes distort according to the pairing model only, whereas

SbV and BiV show both pairing and resonant-bonding JT distortions. Also, unlike in Si, all negatively charged DV defects in Ge are paramagnetic ($S=1$) with C_{3v} symmetry. Our results do not support recent claims that the larger SbV and BiV complexes in Ge adopt the split-vacancy form. We point out that, as a result of the underestimated Ge gap in periodic calculations combined with the local density approximation to the exchange-correlation potential, the energy of split-vacancy structures may be favored due to a strong coupling between the doublet gap state and the host density of states. We show that improved energies may be obtained by carefully choosing the special **k** points to sample the BZ.

The E centers in Ge may occur in four charge states, namely +, 0, −, and =, and the levels shift slightly with the size of the donor impurity. The donor levels are estimated at $\sim E_v+0.1$ eV. This result is based on the recent assignment of a $(0/+)$ level at $E_v+0.095$ eV to SbV,[42] and provides us with an interpretation to four levels at 0.10–0.16 above E_v, reported from early Hall-effect measurements in P, As, Sb, and Bi-doped Ge crystals.[41] First and second acceptor levels are calculated at $\sim E_v+0.3$ eV and $\sim E_c-0.3$ eV, slightly shifting towards lower energies when increasing the mass of the donor atom. These features account well for previously reported measurements.

ACKNOWLEDGMENTS

The authors would like to acknowledge INTAS (Grant No. 03-50-4529), and the FCT in Portugal for financial support. We also thank the Swedish National Infrastructure for Computing (SNIC) under the Swedish Science Council for computer resources.

[1] C. O. Chui, K. Gopalakrishnan, P. B. Griffin, J. D. Plummer, and K. C. Saraswat, Appl. Phys. Lett. **83**, 3275 (2003).
[2] M. L. Lee, E. A. Fitzgerald, M. T. Bulsara, M. T. Currie, and A. Lochtefeld, J. Appl. Phys. **97**, 011101 (2005).
[3] J. Fage-Padersen, A. N. Larsen, and A. Mesli, Phys. Rev. B **62**, 10116 (2000).
[4] H. Haesslein, R. Sielemann, and C. Zistl, Phys. Rev. Lett. **80**, 2626 (1998).
[5] S. Öğüt and J. R. Chelikowsky, Phys. Rev. B **64**, 245206 (2001).
[6] A. Fazzio, A. Janotti, A. J. R. da Silva, and R. Mota, Phys. Rev. B **61**, R2401 (2000).
[7] H. Höhler, N. Atodiresei, K. Schroeder, R. Zeller, and P. H. Dederichs, Phys. Rev. B **71**, 035212 (2005).
[8] J. Coutinho, R. Jones, V. J. B. Torres, M. Barroso, S. Öberg, and P. R. Briddon, J. Phys.: Condens. Matter **17**, L521 (2005).
[9] J. Coutinho, R. Jones, P. R. Briddon, and S. Öberg, Phys. Rev. B **62**, 10824 (2000).
[10] R. Jones, A. Carvalho, J. Coutinho, V. J. B. Torres, S. Öberg, and P. R. Briddon, Solid State Phenom. **108-109**, 697 (2005).
[11] J. Coutinho, V. J. B. Torres, R. Jones, A. Carvalho, S. Öberg, and P. R. Briddon, Appl. Phys. Lett. (to be unpublished).
[12] R. Car, P. J. Kelly, A. Oshiyama, and S. T. Pantelides, Phys. Rev. Lett. **54**, 360 (1985).
[13] M. Werner, H. Mehrer, and H. D. Hochheimer, Phys. Rev. B **32**, 3930 (1985).
[14] G. Vogel, G. Hettich, and H. Mehrer, J. Phys. C **16**, 6197 (1983).
[15] H. Bracht, E. E. Haller, and R. Clark-Phelps, Phys. Rev. Lett. **81**, 393 (1998).
[16] A. Ural, P. B. Griffin, and J. D. Plummer, Phys. Rev. Lett. **83**, 3454 (1999).
[17] M. D. Moreira, R. H. Miwa, and P. Venezuela, Phys. Rev. B **70**, 115215 (2004).
[18] M. I. J. Probert and M. C. Payne, Phys. Rev. B **67**, 075204 (2003).
[19] G. D. Watkins and J. W. Corbett, Phys. Rev. **134**, A1359 (1964).
[20] E. L. Elkin and G. D. Watkins, Phys. Rev. **174**, 881 (1968).
[21] G. D. Watkins, Phys. Rev. B **12**, 4383 (1975).
[22] A. N. Larsen, J. J. Goubet, P. Mejlholm, J. S. Christensen, M. Fanciulli, H. P. Gunnlaugsson, G. Weyer, J. W. Petersen, A. Resende, M. Kaukonen, R. Jones, S. Öberg, P. R. Briddon, B. G. Svensson, J. L. Lindström, and S. Dannefaer, Phys. Rev. B **62**, 4535 (2000).
[23] L. C. Kimerling, H. M. DeAngelis, and C. P. Carnes, Phys. Rev. B **3**, 427 (1971).
[24] G. D. Watkins, Radiat. Eff. Defects Solids **111-112**, 487 (1989).
[25] S. Öğüt and J. R. Chelikowsky, Phys. Rev. Lett. **91**, 235503 (2003).
[26] G. D. Watkins, Physica B **376-377**, 50 (2006).
[27] C. S. Nichols, C. G. Van de Walle, and S. T. Pantelides, Phys. Rev. B **40**, 5484 (1989).
[28] M. Ramamoorthy and S. T. Pantelides, Phys. Rev. Lett. **76**, 4753 (1996).
[29] O. Pankratov, H. Huang, T. Diaz de la Rubia, and C. Mailhiot, Phys. Rev. B **56**, 13172 (1997).
[30] J. Xie and S. P. Chen, Phys. Rev. Lett. **83**, 1795 (1999).
[31] D. C. Mueller, E. Alonso, and W. Fichtner, Phys. Rev. B **68**, 045208 (2003).
[32] D. C. Mueller and W. Fichtner, Phys. Rev. B **70**, 245207 (2004).
[33] M. G. Ganchenkova, A. Yu. Kuznetsov, and R. M. Nieminen, Phys. Rev. B **70**, 115204 (2004).
[34] M. J. Puska, S. Pöykkö, M. Pesola, and R. M. Nieminen, Phys. Rev. B **58**, 1318 (1998).
[35] H. Saito and J. C. Pigg, Bull. Am. Phys. Soc. **9**, 654 (1964).
[36] A. Hiraki, J. W. Cleland, and J. H. Crawford, Jr., in *Radiation Effects in Semiconductors* (Plenum, New York, 1968), p. 224.
[37] A. Colder, M. Levalois, and P. Marie, J. Appl. Phys. **88**, 3082 (2000).
[38] V. P. Markevich, A. R. Peaker, V. V. Litvinov, V. V. Emtsev, and L. I. Murin, J. Appl. Phys. **95**, 4078 (2004).
[39] A. R. Peaker, V. P. Markevich, F. D. Auret, L. Dobaczewski, and N. Abrosimov, J. Phys.: Condens. Matter **17**, S2293 (2005).
[40] V. P. Markevich, I. D. Hawkins, A. R. Peaker, K. V. Emtsev, V. V. Emtsev, V. V. Litvinov, L. I. Murin, and L. Dobaczewski, Phys. Rev. B **70**, 235213 (2004).
[41] V. V. Emtsev, T. V. Mashovets, and S. M. Ryvkin, in *Radiation Damage in Semiconductors*, Inst. Phys. Conf. Ser. No. 16 (London, 1973), p. 17.
[42] C. E. Lindberg, J. Lundsgaard Hansen, P. Bomholt, A. Mesli, K.

Bonde Nielsen, and A. Nylandsted Larsen, Appl. Phys. Lett. **87**, 172103 (2005).
[43] V. A. Telezhkin and K. B. Tolpygo, Fiz. Tverd. Tela (Leningrad) **15**, 1084 (1973) [Sov. Phys. Solid State **15**, 740 (1973)].
[44] P. R. Briddon and R. Jones, Phys. Status Solidi B **217**, 131 (2000).
[45] S. Goedecker, M. Teter, and J. Hutter, Phys. Rev. B **54**, 1703 (1996).
[46] J. P. Perdew and Y. Wang, Phys. Rev. B **45**, 13244 (1992).
[47] C. Hartwigsen, S. Goedecker, and J. Hutter, Phys. Rev. B **58**, 3641 (1998).
[48] J. Donohue, in *The Structures of Elements* (Wiley, New York, 1974).
[49] H. J. McSkimin, J. Appl. Phys. **24**, 988 (1953).
[50] H. J. Monkhorst and J. D. Pack, Phys. Rev. B **13**, 5188 (1976).
[51] A. Resende, R. Jones, S. Öberg, and P. R. Briddon, Phys. Rev. Lett. **82**, 2111 (1999).
[52] J. Coutinho, V. J. B. Torres, R. Jones, and P. R. Briddon, Phys. Rev. B **67**, 035205 (2003).
[53] G. B. Bachelet and N. E. Christensen, Phys. Rev. B **31**, 879 (1985).
[54] S. Zwerdling, B. Lax, L. M. Roth, and K. J. Button, Phys. Rev. **114**, 80 (1959).
[55] G. Makov and M. C. Payne, Phys. Rev. B **51**, 4014 (1995).
[56] J. Lento, J.-L. Mozos, and R. M. Nieminen, J. Phys.: Condens. Matter **14**, 2637 (2002).
[57] M. Saito and A. Oshiyama, Phys. Rev. Lett. **73**, 866 (1994).
[58] J. Coutinho, O. Andersen, L. Dobaczewski, K. B. Nielsen, A. R. Peaker, R. Jones, S. Öberg, and P. R. Briddon, Phys. Rev. B **68**, 184106 (2003).
[59] The $E_{sv}-E_{fv}\sim 80$ meV energies, together with the minute $E_{JT}\sim 50$ meV energies, may be considered as upper bounds for the transformation barriers between (3 C_{1h} pairing structures $+3C_{1h}$ resonant bonding structures) times 2 orientations along $\langle 111\rangle$. This gives a total of 12 accessible orientations.
[60] The gap is given here by the difference between the lowest unoccupied level and the highest occupied level.
[61] The total number of **k** points in MP-2^3 is eight. However, this number reduces to half due to inversion symmetry in the BZ, i.e., the λth eigenvalue at **k**, $E_\lambda(\mathbf{k})$, is equal to $E_\lambda(-\mathbf{k})$. See also Ref. 50.